remote sensing

MDPI

Article

A Parallel Solution of Timing Synchronization in High-Speed Remote Sensing Data Transmission

Fei Teng [1,2], Wenge Yang [1,2], Jining Yan [3], Hongbin Ma [1,2], Yiwen Jiao [1,2,*] and Zefu Gao [1,2]

[1] Department of Electronic and Optical Engineering, Space Engineering University, Beijing 101416, China
[2] Key Laboratory of Intelligent Space TT&C and Operation, Ministry of Education, Beijing 101416, China
[3] School of Computer Science, China University of Geosciences, Wuhan 430078, China
* Correspondence: jiaoyiwen1985@163.com; Tel.: +86-15001361736

Abstract: Considering the problem that the timing synchronization calculation in high-speed remote sensing signal reception is complex and it is difficult for it to be parallel, this paper deduces and designs a parallel timing error estimation and correction scheme. This paper presents the design of polyphase DFT filter banks with non-maximum decimation. The feedforward timing error estimation and correction method is then improved to enhance synchronization performance. Finally, an implementation scheme for parallel timing error estimation and correction is proposed using the polyphase filter bank time domain decomposition method and the filter polyphase model. In the estimation module, the parallel implementation structure of the joint second-order and fourth-order cyclic statistics methods is designed, which improves the estimation accuracy. In the correction module, a fractional delay filtering method with higher accuracy is adopted in order to improve the calibration accuracy and reduce the computational complexity. The timing synchronization of a high-speed remote sensing signal with timing error is simulated and verified. The experimental results show that the parallel method proposed in this paper greatly reduces the processing speed of subband data, and has a good synchronization performance, which is close to the theoretical limit in the demodulation error rate. This paper utilizes a multi-phase DFT filter bank architecture to achieve parallel timing synchronization, which presents a novel approach for the future parallel reception of high-speed remote sensing signals.

Keywords: remote sensing data transmission; timing synchronization; parallel processing; multiphase decomposition

check for updates

Citation: Teng, F.; Yang, W.; Yan, J.; Ma, H.; Jiao, Y.; Gao, Z. A Parallel Solution of Timing Synchronization in High-Speed Remote Sensing Data Transmission. *Remote Sens.* **2022**, *15*, 3347. https://doi.org/10.3390/rs15133347

Academic Editors: Chaowei Yang and Roberto Orosei

Received: 28 March 2023
Revised: 31 May 2023
Accepted: 27 June 2023
Published: 30 June 2023

Copyright: © 2022 by the authors. Licensee MDPI, Basel, Switzerland. This article is an open access article distributed under the terms and conditions of the Creative Commons Attribution (CC BY) license (https://creativecommons.org/licenses/by/4.0/).

1. Introduction

With the increasingly diversified functions and greatly improved resolution of remote sensing satellites [1], the demand for remote sensing data transmission rate has reached tens of Gbps, but the current transmission rate of remote sensing satellites is far from meeting the demand index[2]. The main reason is that, due to its signal processing ability, it is difficult for the ground receiver to process such high-speed remote sensing data in real time, and the operation speed of the traditional serial demodulation module has reached a bottleneck, so it is necessary to design a parallel structure to improve the transmission rate of remote sensing data, and the parallel processing of timing synchronization is an important link.

Among the parallel demodulation methods of high-speed remote sensing signals, the research on frequency domain parallel demodulation architecture based on FFT is relatively mature. In [3], the authors developed a parallel demodulation technology with an APRX structure, which firstly transformed the digital baseband signal into a frequency domain by DFT transform, and then performed parallel matched filtering, parallel timing synchronization, and carrier synchronization, thus greatly reducing the operation speed of the processing chip. In [4], based on APRX architecture, an ASIC chip that can demodulate

a 600 Mbps code rate and is suitable for various modulation modes was developed. In [5], the authors developed a high-speed digital demodulation receiver with QPSK and FQPSK modulation at 600 Mbps. In [6], the author used an ASIC chip with APRX architecture to realize two channels of high-speed data transmission at 1024 Mbps, and the data transmission rate of each channel was 512 Mbps. In [7], the prototype of 800 Mbps fixed-rate 8PSK high-speed demodulation was developed by using APRX parallel architecture. In [8], the authors successfully developed a high-speed demodulator with 1.5 Gbps and 16QAM modulation. In [9], the author developed 64QAM modulation based on APRX architecture, which can realize a high-speed communication demodulation prototype with a 2 Gbps bit rate, and a demodulation error loss of less than 2 dB. In [10], the author further improves the parallel timing and carrier synchronization technology under APRX architecture, and improves the degree of parallelism. In [11], the author improves the timing synchronization technology of a 16QAM modulation system under the APRX framework, saves processing resources, and verifies the communication rate of 1 Gbps at the board level, and the demodulation error loss is within 2 dB. This kind of method has great advantages in reducing hardware processing speed and complexity [12], but, due to the direct use of FFT to realize channelization parallelism, the signal reconstruction performance is not high, resulting in the loss of demodulation performance. The research of parallel demodulation technology based on efficient channelization architecture is still in the theoretical stage. In [13], the authors propose a general scheme of digital demodulation based on polyphase DFT filter bank architecture, which can realize all kinds of filter functions in subbands in parallel, thus greatly reducing the computational complexity.

In the research of the parallel timing synchronization method, the authors in [14] propose a symbol timing correction algorithm for polyphase filter banks. This method uses sampling theorem to derive a method to realize multiple interpolation of received signals in polyphase filter banks, so there is an inherent resolution error in the correction of optimal decision points. In [15], the authors propose a parallel timing correction technology based on a piecewise square algorithm, which can complete timing error correction in parallel. The Gardner error detection algorithm is adopted, and its error detection module and loop filtering module still adopt a serial method. In [9], the author applies the zero-delay second-order cyclic statistics (O&M) algorithm to the feedback loop, and develops parallel structures for the O&M error estimation algorithm and frequency domain timing correction algorithm, respectively. Although the proposed method realizes parallel speed reduction, it is limited to the condition that the symbol oversampling rate is 4. In [13], the authors propose a parallel timing synchronization method using polyphase filter bank technology. The error correction module of this algorithm is based on a technology of simulating the filter by channelized subband factor multiplication, which can realize the function of a fractional delay filter in subbands in parallel, but the performance of this correction method is proportional to the number of channels, so it is difficult to guarantee the accuracy. A parallel timing error estimation technique based on the O&M algorithm is studied in reference [16], and error correction is realized in a frequency domain through DFT operation. This method does not use a feedback control loop, which leads to insufficient timing error estimation accuracy. In [17], the author proposes an interpolation filter for timing error correction using frequency domain filtering technology. The signal is transferred to the frequency domain by an FFT operation, which reduces the processing speed of single-channel signal timing correction. However, this algorithm can only correct a piece of data uniformly, making it unsuitable for cases of fractional symbol oversampling and lacking flexibility. In [18], the author proposes a parallel timing synchronization technology based on APRX architecture, which can achieve synchronization of multiple modulation systems and fractional symbol oversampling. However, its resampling method leads to an increase in computational complexity.

Aiming at the problems of the above methods, such as low synchronization accuracy, poor flexibility, and low parallelism, this paper designs a feedforward parallel timing error estimation and correction technology based on the polyphase DFT filter bank structure to

improve demodulation performance and parallelism. At present, there is no research on parallel timing synchronization of this architecture in the related literature. The architecture proposed in this paper exhibits strong potential for the parallelization of filtering, carrier synchronization, and equalization modules. As a result, it offers the advantages of good flexibility and adaptability, providing a novel approach for the design of multi-mode parallel remote sensing signal receivers.

Section 2 of this paper presents the design of the basic model for parallel demodulation, including the deduction of the implementation structure of polyphase DFT filter banks. The feedforward timing error detection method is also improved to enhance estimation accuracy. Additionally, the implementation structures of the parallel error estimation algorithm and parallel error correction algorithm are derived, and a design scheme is provided. Section 3 verifies the effectiveness of the proposed parallel algorithm using simulation software. Three groups of experiments are conducted to evaluate the performance of the method, with three evaluation indexes used: the relationship between mean square error and signal-to-noise ratio, the relationship between mean square error and roll-off factor, and the bit error rate. Section 4 discusses the comparison of computational complexity between parallel architecture and serial architecture with respect to timing error estimation and timing error correction. Section 5 shows the conclusions.

2. Models and Methods

2.1. Parallel Structure Based on Polyphase DFT Filter Banks

Polyphase DFT filter bank technology can effectively parallelize high-speed serial data streams into multi-channel low-speed data, and the reconstruction performance of the original data is good, so it is suitable for development as a unified parallel structure [19]. The structure of M-channel and D-times decimated cascaded complex exponential filter banks is shown in Figure 1, where $H_m(z)$ and $F_m(z), m = 0, \cdots, M-1$ are band-pass filters. After being filtered by band-pass filters with different gating frequencies, the received remote sensing signals are decimated by D-times. In order to avoid aliasing, $D \leqslant M$ must be met, and then the subband signals are converted to zero frequency by a complex rotator to obtain M-channel subband signals.

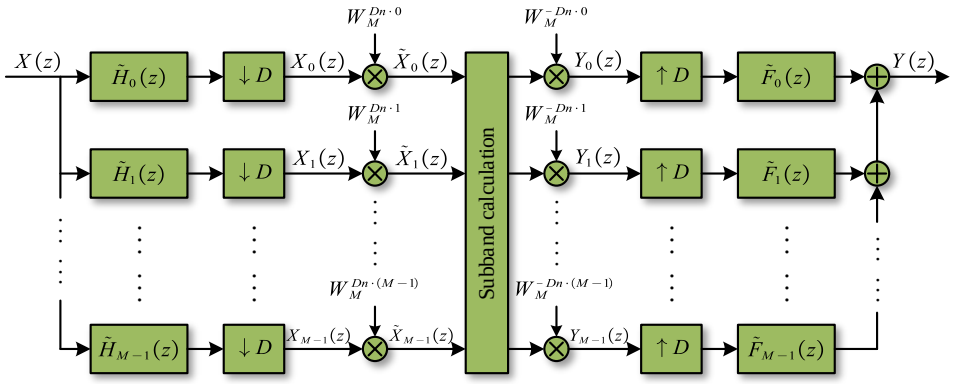


Figure 1. M-channel and D-times decimation complex exponential filter bank model.

It is easy to deduce the expressions of each node signal as follows

$$X_m(z) = \frac{1}{D}\sum_{d=0}^{D-1} X\left(z^{1/D}W_D^d\right) H\left(z^{1/D}W_D^d W_M^m\right) \tag{1}$$

$$\begin{aligned}\tilde{X}_m(z) &= X_m\left(zW_M^{-mD}\right) \\ &= \frac{1}{D}\sum_{d=0}^{D-1} X\left(z^{1/D}W_D^d W_M^{-m}\right) H\left(z^{1/D}W_D^d\right)\end{aligned} \tag{2}$$

$$Y_m(z) = \frac{1}{D}\sum_{d=0}^{D-1} X\left(z^{1/D}W_D^d\right)H\left(z^{1/D}W_M^m W_D^d\right) \tag{3}$$

$$\begin{aligned} Y(z) &= \sum_{m=0}^{M-1} Y_m\left(z^D\right)F(zW_M^m) \\ &= \frac{1}{D}\sum_{d=0}^{D-1}\left[X\left(zW_D^d\right)\cdot\sum_{m=0}^{M-1} H\left(zW_M^m W_D^d\right)F(zW_M^m)\right] \end{aligned} \tag{4}$$

where $W_M = e^{-j2\pi/M}$. In the following, the polyphase realization form of the analysis filter bank is derived, and the prototype filter, $H(z)$, is decomposed by polyphase.

$$\begin{aligned} H(z) &= \sum_{n=-\infty}^{\infty} h(n)z^{-n} \\ &= \sum_{k=0}^{M-1}\left[\sum_{m=-\infty}^{\infty} h(mM+k)z^{-mM}\right]z^{-k} \\ &= \sum_{k=0}^{M-1} H_k\left(z^M\right)z^{-k} \end{aligned} \tag{5}$$

where

$$H_k(z) = \sum_{m=-\infty}^{\infty} h(mM+k)z^{-m} \tag{6}$$

By introducing Formula (5) into Formula (1), we can get

$$\begin{aligned} X_m(z) &= \frac{1}{D}\sum_{d=0}^{D-1} X\left(z^{1/D}W_D^d\right)H\left(z^{1/D}W_D^d W_M^m\right) \\ &= \frac{1}{D}\sum_{d=0}^{D-1}\left[X\left(z^{1/D}W_D^d\right)\sum_{k=0}^{M-1} H_k\left(z^{M/D}W_D^{dM}W_M^{mM}\right)z^{-k/D}W_D^{-kd}W_M^{-km}\right] \end{aligned} \tag{7}$$

When M is an integer multiple of D, then $W_D^{dM} = 1$, so the above formula can be further deformed as follows

$$\begin{aligned} X_m(z) &= \frac{1}{D}\sum_{d=0}^{D-1}\sum_{k=0}^{M-1} X\left(z^{1/D}W_D^d\right)H_k\left(z^{M/D}\right)z^{-k/D}W_D^{-kd}W_M^{-km} \\ &= \frac{1}{D}\sum_{k=0}^{M-1}\left[W_M^{-km}\cdot H_k\left(z^{M/D}\right)\sum_{d=0}^{D-1} X\left(z^{1/D}W_D^d\right)z^{-k/D}W_D^{-kd}\right] \\ &= \sum_{k=0}^{M-1}\left[H_k\left(z^{M/D}\right)\cdot\left[X(z)z^{-k}\right]\big|_{\downarrow D}\cdot W_M^{-km}\right] \end{aligned} \tag{8}$$

where $[\cdot]\big|_{\downarrow D}$ indicates that the sequence is decimated by D times, and, according to the definition of discrete Fourier transform, the accumulation operation in Equation (7) can be realized by IDFT operation, so it can be obtained

$$X_m(z) = M\cdot\mathcal{IDFT}_m\left\{\left[X(z)z^{-m}\right]\big|_{\downarrow D}\cdot H_m\left(z^{M/D}\right)\right\} \tag{9}$$

The derivation method of the polyphase synthesis filter bank is basically the same as that of the analysis end. The polyphase form of the synthesis prototype filter is as follows

$$\begin{aligned} F(z) &= \sum_{n=-\infty}^{\infty} f(n) z^{-n} \\ &= \sum_{k=0}^{M-1} \left[\sum_{m=-\infty}^{\infty} f(mM+k) z^{-mM} \right] z^{-k} \\ &= \sum_{k=0}^{M-1} F_k\left(z^M\right) z^{-k} \end{aligned} \tag{10}$$

where

$$F_k(z) = \sum_{m=-\infty}^{\infty} f(mM+k) z^{-m} \tag{11}$$

By introducing Formula (10) into Formula (4), we can obtain

$$\begin{aligned} Y(z) &= \sum_{m=0}^{M-1} Y_m\left(z^D\right) F(zW_M^m) \\ &= \sum_{m=0}^{M-1} Y_m\left(z^D\right) \sum_{k=0}^{M-1} F_k\left(z^M W_M^{mM}\right) z^{-k} W_M^{-km} \\ &= \sum_{k=0}^{M-1} \left[z^{-k} F_k\left(z^M\right) \cdot \sum_{m=0}^{M-1} Y_m\left(z^D\right) W_M^{-km} \right] \\ &= \sum_{k=0}^{M-1} z^{-k} \left[F_k\left(z^{M/D}\right) \cdot \sum_{m=0}^{M-1} Y_m(z) W_M^{-km} \right] \Big|_{\uparrow D} \\ &= M \cdot \sum_{k=0}^{M-1} z^{-k} \left[F_k\left(z^{M/D}\right) \cdot \mathcal{IDFT}_m\{Y_k(z)\} \right] \Big|_{\uparrow D} \end{aligned} \tag{12}$$

Combining Equations (9) and (12), the structure of a polyphase DFT filter bank with M channels and D times decimation can be obtained, as shown in Figure 2. It is observed that the IFFT operation is utilized at the analysis end and the synthesis end, as the rotation factor indices in Formulas (8) and (12) are both negative, similar to the form of IDFT. The IFFT operation is used solely as a tool to enhance the efficiency of the parallel operation. The structure provides a better scheme for signal parallel speed reduction processing, and the decimation multiple can be adjusted according to the actual situation, as long as the condition that D is divisible by M is met.

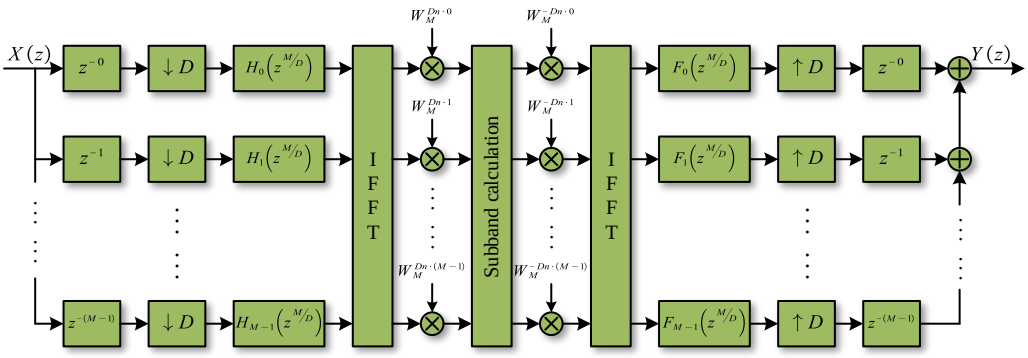


Figure 2. M-channel and D-times decimation polyphase DFT filter bank structure.

When $D = M/2$, the signal can be completely reconstructed, thus ensuring the demodulation performance. Based on this structure, this paper further develops parallel timing synchronization technology to improve the parallelism of high-speed remote sensing data demodulation.

2.2. Basic Principle of Feedforward Timing Error Estimation

Feedforward timing synchronization technology mainly includes two parts: timing error estimation and correction. Because there is no loop filter, the two parts are coupled by a direct cascade to form a complete timing synchronization module, and its basic structure is shown in Figure 3. After receiving the remote sensing signal, it first goes through front-end sampling, frequency conversion, and filtering. Then it is sent to the timing synchronization module, which realizes the estimation and correction of the timing deviation, thus reducing the decision error and improving the accuracy of transmission [20,21]. Finally, it is sent to the back-end processing module to restore the remote sensing image.

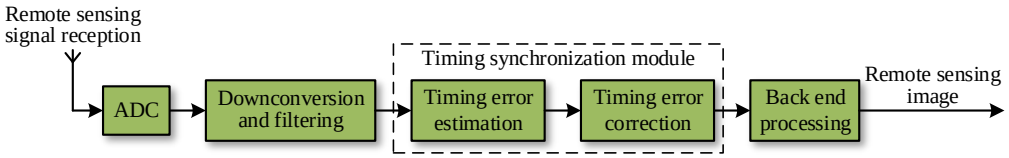


Figure 3. Feedforward timing synchronization structure.

2.2.1. Feedforward Timing Error Estimation Algorithm Based on Second-Order Statistics

For the transmission of on-board remote sensing data, the linear modulation system of raised cosine pulse shaping is usually adopted. At this time, the baseband digital signal obtained by the receiver can be expressed as

$$x_B(n) = \sum_{l=-\infty}^{\infty} \alpha(l) h_c\left(n - lR_f - \mu R_f\right) + v(n) \tag{13}$$

where $\alpha(l)$ is the symbol sequence of the transmitter, $h_c(n)$ stands for convolution of the signal shaping filter and receiving matched filter, which is usually a raised cosine filter in MPSK and QAM modulation systems, $v(n)$ is additive Gaussian noise independent of $\alpha(l)$ with variance N_0, R_f is an oversampling multiple, and $0 \leqslant \mu < 1$ is an unknown timing error, and its range is the time length of one symbol.

When $k = 0, 1, \cdots, R_f - 1$, the second-order cyclic correlation expression of $x_B(n)$ is [22]

$$\begin{aligned} R_{2x}(k;\tau) &= \frac{1}{R_f} \sum_{n=0}^{R_f-1} E\{x_B^*(n) x_B(n+\tau)\} e^{-j2\pi \frac{kn}{R_f}} \\ &= \frac{1}{R_f} e^{j\pi \frac{k\tau}{R_f}} e^{-j2\pi k\mu} G(k;\tau) + N_0 h_c(\tau)\delta(k) \end{aligned} \tag{14}$$

where $x_B^*(n)$ represents the conjugate of complex sequence $x_B(n)$, and $\delta(\cdot)$ is the unit pulse sequence,

$$G(k;\tau) = f_s \int_{-\frac{f_s}{2}}^{\frac{f_s}{2}} H_c\left(f - \frac{kf_p}{2}\right) \cdot H_c\left(f + \frac{kf_p}{2}\right) e^{j2\pi \frac{\tau f}{f_s}} \mathrm{d}f \tag{15}$$

where f_s and f_p are the sampling rate and symbol rate of the digital signal, respectively, and $H_c(\cdot)$ represents the continuous-time Fourier transform of $h_c(t)$.

When $h_c(t)$ is a raised cosine function, it can be obtained from the symmetry property, and $G(k;\tau)$ is a real number, and it is not zero only when $k = 0, \pm 1$. According to Formula (14), when $k = 0$ or $G(k;\tau) = 0$, it does not contribute to the estimation of the timing error, so $k = 1, -1$ must be required. Combining Formulas (14) and (15), it can be deduced that

$$\begin{aligned} R_{2x}^{*}(-k;-\tau) &= \frac{1}{R_f} e^{-j\pi\frac{k\tau}{R_f}} e^{-j2\pi k\mu} G(-k;-\tau) + N_0 h_c(-\tau)\delta(-k) \\ &= \frac{1}{R_f} e^{-j\pi\frac{k\tau}{R_f}} e^{-j2\pi k\mu} G(k;\tau) + N_0 h_c(\tau)\delta(k) \\ &= e^{-j2\pi\frac{k\tau}{R_f}} R_{2x}(k;\tau) \end{aligned} \tag{16}$$

Equation (16) shows that all cyclic correlations of $R_{2x}(-1;\tau)$ can be expressed by $R_{2x}(1;\tau)$, so it is only necessary to consider the case of $k = 1$.

When the number of observation samples is N_s, the expression of the asymptotic unbiased estimation value of the second-order cyclic correlation is [23,24]

$$\hat{R}_{2x}(1;\tau) = \frac{1}{N_s} \sum_{n=0}^{N_s-\tau-1} x_B^{*}(n) x_B(n+\tau) e^{-j2\pi\frac{n}{R_f}}, \tau \geqslant 0 \tag{17}$$

Combining Equations (14) and (17), we can obtain the expression of timing estimation based on second-order cyclic correlation as follows

$$\hat{\mu} = -\frac{1}{2\pi} \arg\left\{ \hat{R}_{2x}(1;\tau) e^{-j\pi\frac{\tau}{R_f}} \right\} \tag{18}$$

2.2.2. Derivation of Feedforward Timing Estimation Algorithm Combining Second-Order and Fourth-Order Statistics

In this paper, the timing estimation algorithm based on joint second-order and fourth-order statistics is adopted [25], and its parallel implementation structure is designed. At the cost of increasing a little computational complexity, the mean square error performance of this algorithm is better than that of two separate algorithms under different signal-to-noise ratios and different shaping roll-off factors. The estimation expression of timing synchronization error μ is

$$\hat{\mu} = -\frac{1}{2\pi} \arg\left\{ \boldsymbol{\alpha}^{\mathrm{T}} \hat{\mathbf{R}}_x \right\} \tag{19}$$

where

$$\begin{aligned} \boldsymbol{\alpha} &:= [1 \alpha_1]^{\mathrm{T}} \\ \hat{\mathbf{R}}_x &:= \left[\hat{R}_{2x}(1;0) \ \hat{R}_{4x}(1;0,0,0) \right]^{\mathrm{T}} \end{aligned} \tag{20}$$

$\hat{R}_{2x}(1;0)$ and $\hat{R}_{4x}(1;0,0,0)$ are the second-order and fourth-order cyclic correlation zero-delay sample estimates of the transmission signal, respectively, and the expressions are as follows

$$\begin{aligned} \hat{R}_{2x}(1;0) &= \frac{1}{N_s} \sum_{n=0}^{N_s-1} |x_B(n)|^2 e^{-j2\pi\frac{n}{R_f}} \\ \hat{R}_{4x}(1;0,0,0) &= \frac{1}{N_s} \sum_{n=0}^{N_s-1} |x_B(n)|^4 e^{-j2\pi\frac{n}{R_f}} \end{aligned} \tag{21}$$

When the shaping roll-off factor and signal-to-noise ratio of the transmission signal change, the mean square error of the estimation is minimized by selecting different values of parameter α_1, and the solution is given by Equation (22).

$$\hat{\alpha}_1 = \frac{[01] \cdot \left[\boldsymbol{\Pi} - \mathrm{re}\left(e^{j4\pi\mu} \tilde{\boldsymbol{\Pi}} \right) \right]^{-1} \boldsymbol{\beta}}{[10] \cdot \left[\boldsymbol{\Pi} - \mathrm{re}\left(e^{j4\pi\mu} \tilde{\boldsymbol{\Pi}} \right) \right]^{-1} \boldsymbol{\beta}} \tag{22}$$

where

$$\begin{aligned}\mathbf{\Pi} &= \lim_{N_s\to\infty} N_s \mathrm{E}\left\{ \left[\hat{R}_{2x} - R_{2x}\ \hat{R}_{4x} - R_{4x}\right] \cdot \left[\hat{R}_{2x} - R_{2x}\ \hat{R}_{4x} - R_{4x}\right]^{\mathrm{H}} \right\} \\ \tilde{\mathbf{\Pi}} &= \lim_{N_s\to\infty} N_s \mathrm{E}\left\{ \left[\hat{R}_{2x} - R_{2x}\ \hat{R}_{4x} - R_{4x}\right] \cdot \left[\hat{R}_{2x} - R_{2x}\ \hat{R}_{4x} - R_{4x}\right]^{\mathrm{T}} \right\}\end{aligned} \tag{23}$$

$$\boldsymbol{\beta} = \left[\frac{\rho}{8}\ Q(1;0)\right]^{\mathrm{T}} \tag{24}$$

where ρ is the roll-off factor of the signal shaping filter. By combining Formulas (14) and (15), the following can be obtained

$$\begin{aligned}R_{2x}(1;0) &= \frac{\rho}{8} e^{-j2\pi\mu} \\ R_{4x}(1;0,0,0) &= Q(1;0) e^{-j2\pi\mu}\end{aligned} \tag{25}$$

where

$$Q(1;0) = \frac{\kappa}{R_f} \int_{-1/2}^{1/2} H_{rc}^2(f) H_{rc}^2\left(f + \frac{1}{R_f}\right) df + \frac{\rho}{2}\left(\frac{4-\rho}{4} + \sigma_v^2\right) \tag{26}$$

where κ is the sample kurtosis of the MPSK modulation sequence, σ_v^2 is the variance of zero-mean Gaussian white noise, and $H_{rc}^2(f)$ satisfies the following equation.

$$H_{rc}^2(f) = e^{j2\pi\mu R_f f} \cdot \mathcal{F}\left\{h_c^2(n)\right\} \tag{27}$$

where $\mathcal{F}\{\cdot\}$ stands for Fourier transform.

For the case of remote sensing data transmission mainly considered in this paper, the satellite-ground wireless communication link is involved. Therefore, the signal-to-noise ratio of the received signal is usually low, that is, σ_v^2 is relatively large. Through calculation, the α_1 value that meets the conditions is -0.0880, which can be obtained by bringing it into Equation (19) and sorting it out.

$$\hat{\mu} = -\frac{1}{2\pi}\arg\left\{ \frac{1}{N_s} \sum_{n=0}^{N_s-1} \left[|x_B(n)|^2 - 0.1326 |x_B(n)|^4 \right] \cdot e^{-j2\pi \frac{n}{R_f}} \right\} \tag{28}$$

2.3. Parallel Design of Joint Second-Order and Fourth-Order Statistics Timing Estimation

According to Formula (12), the following can be obtained

$$Y(z) = M \cdot \sum_{k=0}^{M-1} z^{-k} S_k\left(z^D\right) \tag{29}$$

where $S_k(z)$ represents the result of the k-th subband signal after IFFT transform and comprehensive filtering. In order to derive the implementation structure of the parallel timing error estimation, the above formula is expressed in the time domain as

$$y(n) = M \cdot \sum_{k=0}^{M-1} s_k'(n-k) \tag{30}$$

where $s_k'(n)$ is the result of D times interpolation of $S_k(z)$'s inverse Fourier transform $s_k(m)$, and discrete time variables m and n, respectively, represent the time rates before and after interpolation, and the time domain relationship before and after interpolation is as follows

$$s_k'(n) = \begin{cases} s_k(m), & n = mD \\ 0, & \text{else} \end{cases} \tag{31}$$

As can be seen from Equation (31), the value of the subband signal $s'_k(n)$ is 0 at most times. Let $n = iD + m$, $i = 0, 1, \cdots \infty, m = 0, 1, \cdots, D-1$, then Equation (30) can be transformed into

$$\begin{aligned} y(n) &= y(iD + l) \\ &= M \cdot \sum_{k=0}^{M-1} s'_k(iD + l - k) \\ &= M \cdot [s_l(i) + s_{l+D}(i-1)] \end{aligned} \tag{32}$$

Combining Equations (28) and (32), the block diagram of parallel timing error estimation with an efficient channelization structure can be obtained, as shown in Figure 4. It can be seen from the figure that the purpose of parallel deceleration is achieved by transferring the square operation and the quartic operation to the subband, and the operating rate of each module is consistent with the signal rate of a single channel, so the subband processing rate can be adjusted by flexibly adjusting the number of channels.

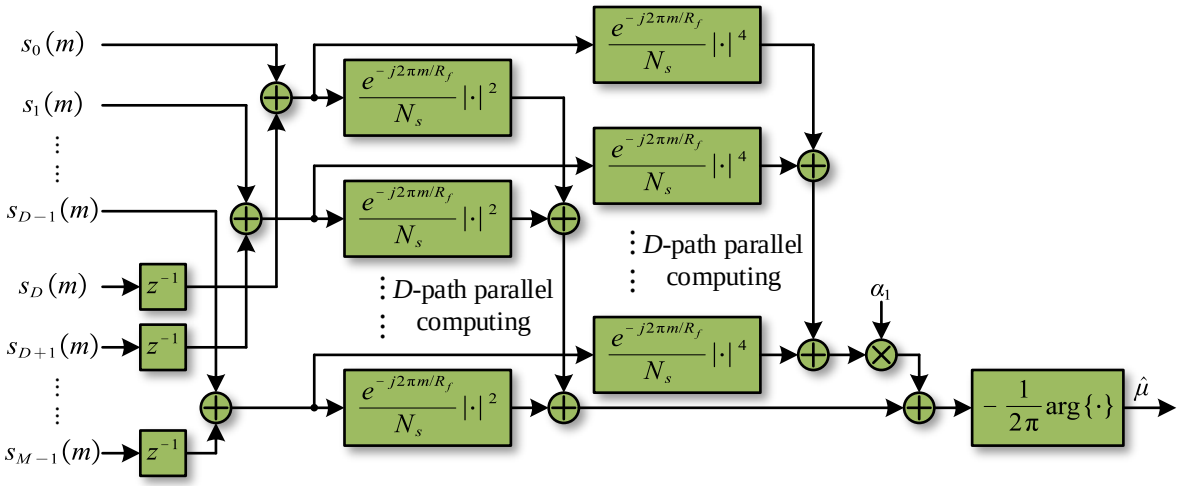


Figure 4. Block diagram of parallel timing error estimation for efficient channelized structure.

2.4. Design of Parallel Timing Correction Scheme

After the timing error estimation process is completed, it is necessary to use a fractional delay filter to interpolate the sampling samples, in order to realize the timing error correction. By adding a rectangular window to the ideal low-pass filter, a fractional delay filter with good performance can be obtained. Let the filter order be L_D, and its coefficient expression is

$$l(n) = \sin c(\pi n - \hat{\mu}_\lambda f_p), n = -\frac{L_D}{2} + 1, \cdots, \frac{L_D}{2} \tag{33}$$

where $\hat{\mu}_\lambda$ is the timing estimation error at different decision moments, λ is the pointer of the sample to be corrected, and its value range is $\lambda \in [0, L_E - 1]$, and L_E is the sample observation length of the estimator. When the oversampling rate, R_f, is an integer, $\hat{\mu}_\lambda$ is considered to be a fixed value in the observation period, and when R_f is not an integer, $\hat{\mu}_\lambda$ changes periodically, and its expression is

$$\hat{\mu}_\lambda = \hat{\mu} + k_p \frac{f_s}{f_p} - \lambda \tag{34}$$

where $k_p = 0, 1, \cdots$ is the decision point to be corrected, and for each k_p, the sample pointer, λ, must satisfy the following inequality

$$\frac{\lambda}{f_s} \leqslant \frac{k_p}{f_p} < \frac{\lambda + 1}{f_s} \tag{35}$$

Next, the parallel timing error correction algorithm based on an efficient channelization structure is derived, and the synthesized signal, $Y(z)$, is corrected. Let the fractional delay filter be $L(z)$, and the filtered signal, $Y_e(z)$, can be obtained according to Equation (29).

$$\begin{aligned} Y_e(z) &= Y(z)L(z) \\ &= \sum_{k=0}^{M-1} S_k\left(z^D\right) L(z) z^{-k} \end{aligned} \tag{36}$$

In order to realize $L(z)$ in parallel, it is polyphase decomposed

$$\begin{cases} L(z) = \sum\limits_{i=0}^{L_D-1} L_i\left(z^{L_D}\right) z^{-i} \\ L_i(z) = \sum\limits_{d=-\infty}^{\infty} l(dL_D + i) z^{-d} \end{cases} \tag{37}$$

When D can be divisible by L_D, Equation (37) is brought into Equation (36) to obtain

$$\begin{aligned} Y_e(z) &= \sum_{k=0}^{M-1} S_k\left(z^D\right) \left[\sum_{i=0}^{L_D-1} L_i\left(z^{L_D}\right) z^{-i}\right] z^{-k} \\ &= \sum_{k=0}^{M-1} \left[\sum_{i=0}^{L_D-1} S_k\left(z^D\right) L_i\left(z^{L_D}\right) z^{-i}\right] z^{-k} \\ &= \sum_{k=0}^{M-1} \sum_{i=0}^{L_D-1} \left[S_k\left(z^{D/L_D}\right) L_i(z)\right]\big|_{\uparrow L_D} \cdot z^{-(i+k)} \end{aligned} \tag{38}$$

Equation (38) moves the fractional delay filter before the interpolator by polyphase decomposition, which reduces the operation speed. The implementation structure of the parallel timing error correction is derived below. As can be seen from Equation (37), after the fractional delay filter, $L(z)$, is polyphase decomposed, the data length of $L_i(z)$ is 1, so Equation (38) can be expressed as

$$y_e(n) = \sum_{k=0}^{M-1} \sum_{i=0}^{L_D-1} \left[l(i) s'_k(n-k-i)\right] \tag{39}$$

Let $n = pD + q$, $p \in \mathrm{Z}, q = 0, 1, \cdots, D-1$, where Z represents the set of all integers, then the above formula can be transformed into

$$\begin{aligned} y_e(n) &= y_e(pD+q) \\ &= \sum_{k=0}^{M-1} \sum_{i=0}^{L_D-1} \left[l(i) s'_k(pD+q-k-i)\right] \end{aligned} \tag{40}$$

According to Formula (31), only when $pD + q - k - i$ is an integer multiple of D, the above formula is not zero, so $k + i = q + rD$, $r \in \mathrm{Z}$ can be set, then we can obtain

$$\begin{aligned} y_e(n) = \sum_{\substack{k+i=q+rD \\ k\in[0,M-1], i\in[0,L_D-1]}} \left[l(i) s_k(p-r)\right] \end{aligned} \tag{41}$$

For the 2-times oversampling channelization structure adopted in this paper, $0 \leqslant k + i \leqslant 3D - 2$, so

$$-1 + \frac{1}{D} \leqslant r = \frac{k+i-q}{D} \leqslant 3 - \frac{2}{D} \tag{42}$$

Since r is an integer, r = 0, 1 or 2. This shows that it takes, at most, 3 subband data to complete a convolution operation, which is the delay caused by the fractional delay filter and non-maximum decimation structure.

Taking $M = 8, D = L_D = 4$ as an example, Figure 5 shows the schematic diagram of the calculation rules using the parallel timing error correction method proposed in this paper. It can be seen that each convolution calculation is obtained by multiplying the data of eight channels at a certain time by the corresponding filter factors and adding them. It should be pointed out that the final sampling decision process only needs to obtain the result of delay correction of a certain fraction at a certain point, so the polyphase filtering calculation for $L(z)$ does not need to be completed; only the product operation is needed for the sampling points at the decision time, and the ratio of the multiplication operation frequency to the symbol rate is L_D/D.

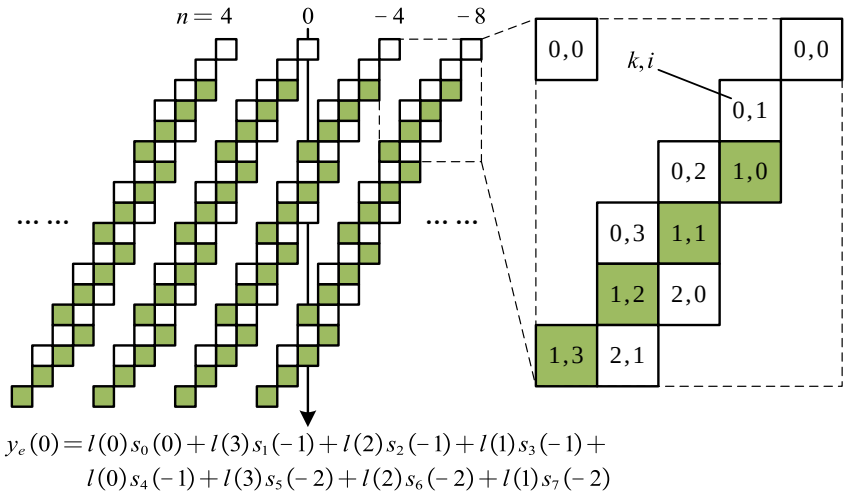


Figure 5. Schematic diagram of parallel timing correction calculation rules.

According to Equation (41), the block diagram of parallel timing error correction based on the efficient channelization structure can be obtained, as shown in Figure 6.

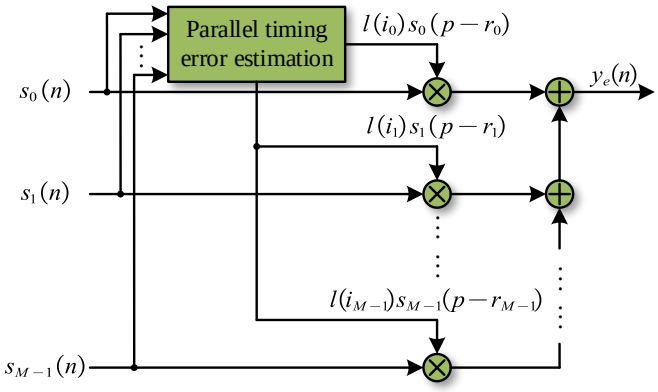


Figure 6. Block diagram of parallel timing error correction for efficient channelized structure.

The parallel signal filtered by the comprehensive filter is firstly estimated for timing error, and the calculated estimated value, $\hat{\mu}$, is brought into Equations (33) and (34) to obtain the fractional delay filter, and then the correction factor of each channel is calculated according to the time, λ, of the point to be interpolated, and the corrected decision data can be obtained only by multiplying once every symbol interval.

3. Results

This section uses computer simulation to verify the effectiveness of the above design. The timing deviation involved in high-speed remote sensing data transmission is processed in parallel synchronization, and the performance of this algorithm is compared with that of common algorithms [26]. M-QAM or M-PSK modulation is usually used in high-speed

remote sensing data transmission systems. Considering the high loss of satellite-to-ground transmission links and the limited transmission power on the satellite, this experiment adopts the QPSK modulation system with a high power utilization rate. The specific simulation parameters are shown in Table 1, where T_p represents the time interval of one symbol. In this simulation, an analog signal with a specific timing error is initially generated using Formula (13). Subsequently, both the square-law algorithm and the improved algorithm are employed to estimate and correct the timing error, respectively, thereby validating the performance of the improved algorithm. The Monte Carlo method is used to simulate the improved estimator and the traditional estimator for 10^6 times, and three comparative experiments are carried out, respectively.

Table 1. Setting of simulation parameters.

Modulation System	**Oversampling Rate (R_f)**	**Roll off Factor (β_c)**
QPSK	4	0.2
Timing Error	**Observation Length**	**Number of Simulated Samples**
$0.3/T_p$	$100T_p$	10^6

Experiment 1: Comparison of mean square error (MSE) and signal-to-noise ratio (SNR) curve between the parallel estimation algorithm and classical algorithm. Figure 7 shows that the MSE of the proposed parallel estimation algorithm is compared with that of the commonly used second-order algorithm when the SNR is 0–20 dB. The green curve in the figure is the MSE-SNR curve calculated by the O&M algorithm, and the estimation performance of this algorithm is not weaker than that of most improved algorithms at $R_f = 4$ [25]. The red curve is the parallel estimation algorithm. The blue curve is a modified Cramero bound, and its expression is

$$\mathrm{MCRB}(\hat{\mu}) = \frac{R_f}{8\pi^2 N_s \xi \mathrm{SNR}} \tag{43}$$

In the case of raised cosine pulse shaping, the parameter ξ is expressed as

$$\xi = \frac{1}{12} + \beta_c^2 \left(0.25 - \frac{2}{\pi^2}\right) \tag{44}$$

The experimental results show that the estimation performance of the improved method is better than the traditional algorithm under different SNR, and in the parallel architecture designed in this paper the calculation amount of the zero-offset fourth-order statistics is acceptable.

Experiment 2: Comparison of MSE and roll-off factor curve between the parallel estimation algorithm and classical algorithm. Figure 8 shows the curve of the MSE between the parallel algorithm and the traditional algorithm varying with the roll-off factor when the signal-to-noise ratio is 20 dB. The experimental results show that the estimation performance of the improved algorithm is better than that of the second-order algorithm under different β_c conditions, and the smaller β_c is, the more obvious is the advantage.

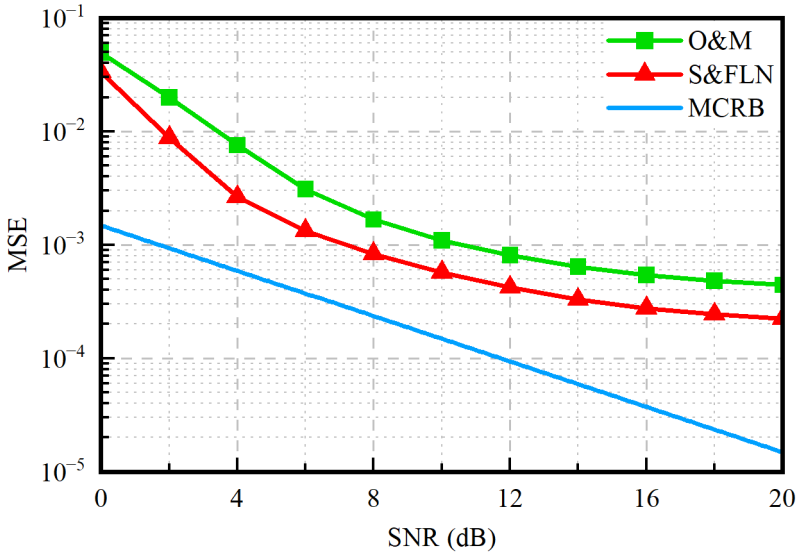


Figure 7. The curve of MSE with SNR for two methods.

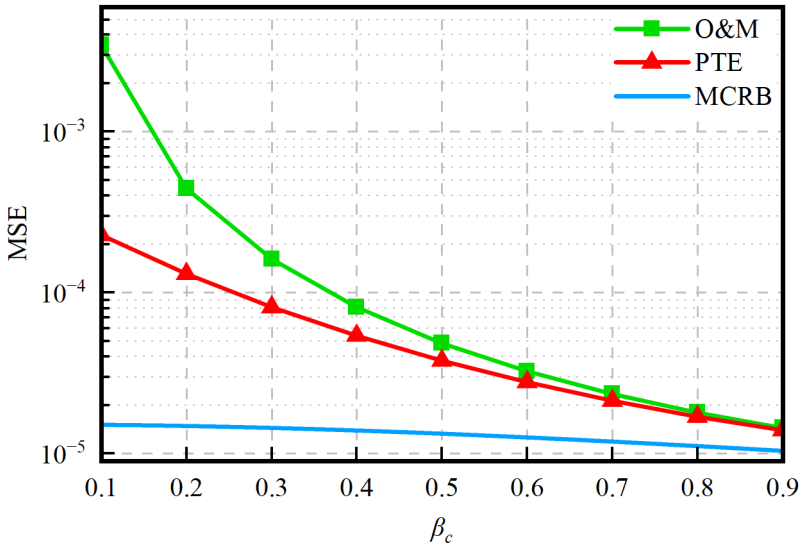
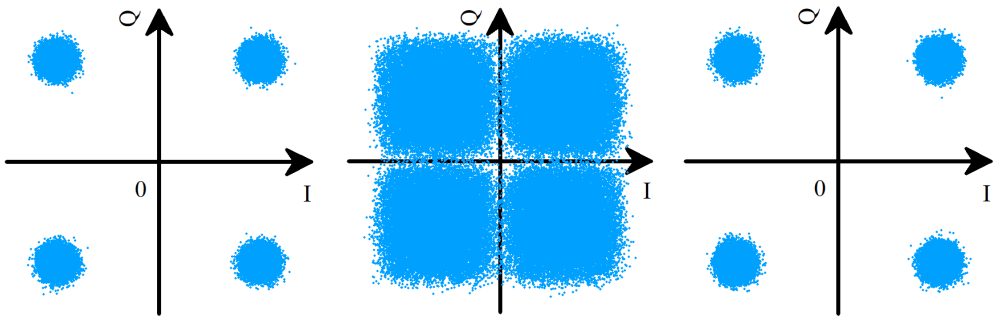


Figure 8. The curve of MSE with β_c for two methods.

Experiment 3: Performance comparison between the parallel error correction algorithm and square interpolation algorithm. The analog signal generated by Formula (13) is demodulated directly to obtain the demodulated data. The performance of the improved algorithm can be assessed by comparing the bit error rate indicators after demodulation. Figure 9 shows that when the signal-to-noise ratio is 20 dB: (a) there is no timing error; (b) there is a timing error of $\mu = 0.25$, and (c) using the demodulation constellation diagram after this parallel synchronization, it can be seen from the diagram that the parallel timing synchronization technology designed in this paper has good synchronization performance for QPSK signals.



(a) Constellation without timing error (b) Constellation with timing error (c) Constellation after timing synchronization

Figure 9. Comparison of constellation diagrams before and after timing error correction.

Next, the performance of the demodulation error rate is simulated and compared. Figure 10 shows the demodulation error rate curve of the parallel timing method and the traditional method when the signal-to-noise ratio is 6–10 dB. The blue curve in the figure is a theoretical curve. The theoretical bit error rate, P_b, of QPSK modulation is

$$P_b = \frac{1}{2}\mathrm{erfc}\left(\sqrt{\frac{E_b}{N_0}}\right) \tag{45}$$

where E_b is the average energy per bit, N_0 is the noise power spectral density, and $\mathrm{erfc}(\cdot)$ is the complementary error function, defined as

$$\mathrm{erfc}(x) = \frac{2}{\sqrt{\pi}}\int_x^{\infty} e^{-\eta^2} d\eta \tag{46}$$

The red curve is the bit error rate curve demodulated by the improved parallel timing synchronization method in this paper, and the green curve is the bit error rate curve of the traditional method. The experimental results show that the improved parallel timing synchronization method is superior to the traditional method in the performance of error demodulation, and has a good application prospect.

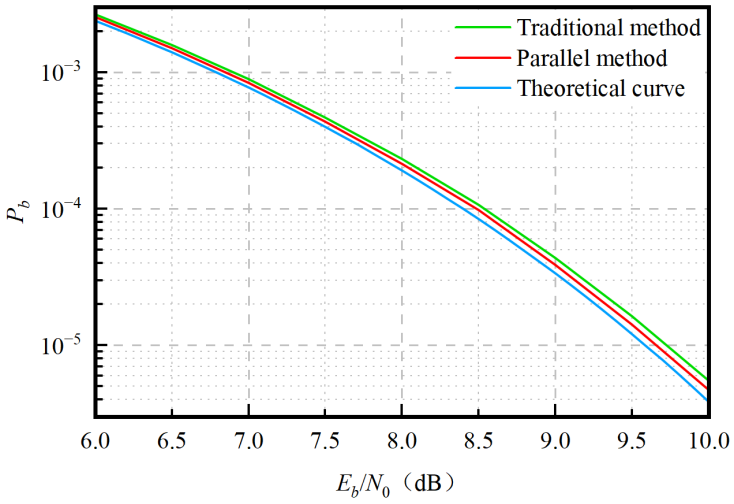


Figure 10. Demodulation error rate curves of two methods.

Finally, we present a performance comparison between the traditional method and the improved method. Table 2 illustrates the comparison of estimation performance, demodulation performance, and data rate. It is evident that the proposed improved algorithm

outperforms the traditional algorithm in terms of timing error estimation performance and demodulation error performance. Moreover, the designed parallel structure can significantly decrease the data processing rate of high-speed remote sensing signals, which is highly beneficial for achieving real-time demodulation.

Table 2. Performance comparison between traditional method and improved method.

Evaluating indicator & Method	Traditional Method	Improved Method
Mean square error of timing error estimation	4.36×10^{-2} (SNR = 0 dB) 1.10×10^{-3} (SNR = 10 dB) 4.44×10^{-4} (SNR = 20 dB) comparatively large	3.33×10^{-2} (SNR = 0 dB) 5.73×10^{-4} (SNR = 10 dB) 2.22×10^{-4} (SNR = 20 dB) reduced by 1–3 dB
Demodulation error rate after timing synchronization (SNR = 10 dB)	5.12×10^{-6}	4.72×10^{-6} (reduced by 0.36 dB)
Single channel data rate	$= f_s$	$= 1/D \cdot f_s$

4. Discussion

This section discusses the comparison of computation complexity between parallel architecture and serial architecture, in order to show the advantages of parallel architecture in high-speed remote sensing signal transmission [27,28].

4.1. Analysis of Computational Complexity for Parallel Timing Error Estimation Algorithm

The calculation of the traditional second-order statistics timing error estimation algorithm is relatively simple. According to Equations (17) and (18), the traditional estimation algorithm squares the collected digital signal streams one by one, and the calculation amount of this step is that all sampled data are multiplied once. After accumulating a certain amount of observed data, the results of these squares are averaged, and the offset phase value is obtained using the complex angular algorithm. The main calculation is the multiplication operation synchronized with the sampling data rate and the calculation of the radiation angle after accumulating certain observations.

In this paper, the traditional second-order statistics algorithm is improved. By introducing the joint second-order and fourth-order statistics, the performance of the timing error estimation is improved, and the calculation amount is increased to some extent. According to Equations (19)–(21), the improved algorithm not only calculates the square of the sampled data, but also calculates their quartic power, so there is one more multiplication operation. After accumulating the observed data, the results of the square and quartic power are averaged, respectively, and then the angle calculation operation is carried out after weighted addition. Because each calculation of the radiation angle is carried out after a certain cumulative observation, its calculation rate is much lower than the sampling data rate. Therefore, the burden caused by the weighted addition operation of the improved algorithm can be ignored. The main calculation amount of the improved algorithm is the multiplication operation of twice the sampling data rate and the calculation of the radiation angle after accumulating certain observations.

At present, the data rate of high-speed remote sensing signals transmitted to the receiving end reaches several Gbps, which puts great pressure on to the digital processing module. The parallel processing algorithm proposed in this paper can effectively reduce the processing rate of single-channel signals. Let us consider its single-channel computational complexity. Assuming that the number of parallel channels is M and the decimation multiple is $1/2M$, the data rate of each subband signal is $2/M$ of the total rate. The improved timing error estimation algorithm is used to calculate, and the main calculation of a single channel is the multiplication operation of $4/M$ times the sampling data rate and the calculation of the divergence angle after accumulating certain observations. Obviously, with the increase of the number of channels, the processing rate of single-channel signals will decrease proportionally. In practical application, the number of channels, M, can be

reasonably selected according to the transmission rate of remote sensing signals and the hardware processing capacity, thus reducing the demodulation pressure of the receiver.

4.2. Analysis of Computational Complexity for Parallel Timing Correction Algorithm

Traditional timing error correction algorithms mainly include the square interpolation method and fractional delay filtering method. The square interpolation method is simple in calculation, but the correction accuracy is low, so this paper adopts the fractional delay filtering method with its higher accuracy.[29] When the order of the fractional delay filter is L_D, the number of multipliers required for one filtering operation is L_D. However, for timing correction, it is not necessary to filter all the sampled data, but only the data at the decision time, that is, the calculation rate of filtering is the same as the symbol rate. When the symbol oversampling rate of the system is R_f, the calculation amount of the serial timing correction algorithm is the number of multiplication operations that are L_D/R_f times the sampling data rate.

In this paper, the operation of fractional delay filtering is designed in parallel using polyphase decomposition technology. According to Equation (41), the multiplication calculation rate of the timing correction for each subband is $\left(L_D/R_f\right) \cdot (2/M)$ times the sampling data rate. When the number of channels increases, the calculation rate of the parallel timing correction decreases proportionally, and the expected speed reduction effect is achieved.

5. Conclusions

To address the challenge of the extensive computational requirements and complex parallel implementation of timing synchronization, this paper proposes an efficient parallel computing scheme. Specifically, we derive and design a parallel timing estimation structure and a parallel timing correction structure under the efficient channelization architecture. The parallel implementation structure of timing error estimation is obtained by utilizing the time-domain expression of polyphase synthesis filter banks, where the computation of each parallel branch requires only two multiplications. The parallel timing error correction structure under the filter bank architecture is derived using polyphase decomposition technology. By decimating the fractional delay filter, we obtain the weighting factors of each branch, enabling the multiplier to replace the filter with high computational complexity. This approach significantly reduces the processing speed and improves the demodulation rate of the receiver receiving high-speed remote sensing signals. The simulation results show that the mean square error of the improved parallel timing error estimation algorithm is lower than that of the traditional algorithm, and the demodulation performance of the overall timing synchronization algorithm is close to the theoretical limit. In the parallel structure, the processing rate of the single-channel signal is obviously reduced, and the calculation rate can be controlled within an acceptable range by flexibly setting the number of channels. The research presented in this paper offers a novel architecture for the parallel demodulation of high-speed remote sensing signals. This architecture is highly scalable and well-suited for the development and research of multi-mode parallel receivers in the future.

Author Contributions: Conceptualization, F.T., W.Y. and Y.J.; data curation, H.M. and Z.G.; formal analysis, F.T. and Y.J.; funding acquisition, W.Y., H.M. and Y.J.; investigation, F.T. and Z.G.; methodology, F.T., J.Y. and W.Y.; project administration, J.Y., H.M. and Z.G.; resources, J.Y. and H.M.; software, F.T.; supervision, W.Y. and Y.J.; validation, J.Y.; visualization, Z.G.; writing—original draft, F.T.; writing—review and editing, W.Y., J.Y., H.M. and Y.J. All authors have read and agreed to the published version of the manuscript.

Funding: This research was funded by Major Science and technology Projects of Beijing under Grant Z181100002918004.

Data Availability Statement: Not applicable.

Acknowledgments: The authors would like to thank the editor and anonymous reviewers for their valuable comments and suggestion.

Conflicts of Interest: The authors declared no potential conflicts of interest with respect to the research, authorship, and/or publication of this article.

References

1. Zhou, Y. Discussion on the Development of Remote Sensing Satellite Data Transmission Technology. *China Plant Eng.* **2022**, *2*, 194–195.
2. Wang, Q.; Li, W.; Yu, Z.; Abbasi, Q.; Imran, M.; Ansari, S.; Sambo, Y.; Wu, L.; Li, Q.; Zhu, T. An Overview of Emergency Communication Networks. *Remote Sens.* **2023**, *15*, 1595. [CrossRef]
3. Srinivasan, M.; Chen, C.C.; Grebowsky, G.; Gray, A. An all-digital, high data-rate parallel receiver. *Jpl Tda Prog. Rep.* **1997**, *42*, 131.
4. Ghuman, P.; Sheikh, S.; Koubek, S.; Hoy, S.; Gray, A. High Rate Digital Demodulator ASIC. In Proceedings of the 34th International Telemetering Conference, Town & Country Resort Hotel and Convention Center, San Diego, CA, USA, 26–29 October 1998.
5. Gray, A.; Srinivasan, M.; Simon, M.; Yan, T.Y. Flexible all-digital receiver for bandwidth efficient modulations. In Proceedings of the 35th International Telemetering Conference, Riviera Hotel and Convention Center, Las Vegas, NA, USA, 25–28 October 1999.
6. Springett, J.C. Achieving future space very long baseline interferometry gigabits-per-second data rates. In *The Interplanetary Network Progress Report 42–149*; NASA: Washington, DC, USA, 2002; pp. 1–26. Available online: https://ipnpr.jpl.nasa.gov (accessed on 27 March 2023).
7. Liang, X. Research and Implementation of Matched Filtering and Timing Recovery for 800 Mbps High-Speed Data Transmission Receiver. Master's Thesis, National University of Defense Technology, Changsha, China, 2007.
8. Guo, X.F.; Zheng, X.F.; Lu, M.H.; Li, Y.H. Design and application of high-speed data transmission QAM demodulator. *J. Telem. Track. Command.* **2011**, *32*, 21–25.
9. Lin, C.X. Research on Demodulation Technique and Its Implementation for 2 Gbps High Speed Communication. Ph.D. Thesis, Tsinghua University, Beijing, China, 2012.
10. Zeng, H. Research on Demodulation Techniques Based on A Parallel All-digital Receiving Structure Named as APRX. Master's Thesis, University of Electronic Science and Technology of China, Chengdu, China, 2013.
11. Cui, L.B. Research on Parallel Timing Synchronization Technology in QAM Demodulation Data. Master's Thesis, University of Electronic Science and Technology of China, Chengdu, China, 2018.
12. Wang, Z.; Song, Y.; Li, Y. Ultra-Wideband Imaging via Frequency Diverse Array with Low Sampling Rate. *Remote Sens.* **2022**, *14*, 1271. [CrossRef]
13. Chen, X.; Venosa, E.; Rao, B.D. Non-maximally decimated filter bank-based single-carrier receiver: A pathway to next-generation wideband communication. *Eurasip J. Adv. Signal Process.* **2014**, *2014*, 1–15. [CrossRef]
14. Harris, F.J.; Rice, M. Multirate digital filters for symbol timing synchronization in software defined radios. *IEEE J. Sel. Areas Commun.* **2001**, *19*, 2346–2357. [CrossRef]
15. Schmidt, D.; Lankl, B. Parallel architecture of an all digital timing recovery scheme for high speed receivers. In Proceedings of the 2010 7th International Symposium on Communication Systems, Networks & Digital Signal Processing (CSNDSP 2010), Newcastle Upon Tyne, UK, 21–23 July 2010; pp. 31–34.
16. Xiao, L. Study and Implementation of Synchronization for Parallel High Data Rate Demodulation System. Master's Thesis, University of Electronic Science and Technology of China, Chengdu, China, 2017.
17. Wang, C.H. Design and Implementation of High Speed Parallel Interpolation Filter Based on FPGA. Master's Thesis, Chengdu University of Technology, Chengdu, China, 2021.
18. Li, Z. The research and Implementation of Symbol Variable Rate Timing Synchronization for Wideband Satellite. Master's Thesis, Xidian University, Xi'an, China, 2022.
19. Teng, F.; Jiao, Y.; Yang, W.; Yan, J.; Gao, Z.; Lu, Z. Multiphase Parallel Demodulation for Remote Sensing Satellite Data Transmission–Filter Bank Based on WOLA Structure. *IEEE J. Sel. Top. Appl. Earth Obs. Remote. Sens.* **2022**, *15*, 9556–9565. [CrossRef]
20. Morge-Rollet, L.; Le Jeune, D.; Le Roy, F.; Canaff, C.; Gautier, R. From Modeling to Sensing of Micro-Doppler in Radio Communications. *Remote Sens.* **2022**, *14*, 6310. [CrossRef]
21. Schlüter, M.; Dörpinghaus, M.; Fettweis, G.P. Bounds on phase, frequency, and timing synchronization in fully digital receivers with 1-bit quantization and oversampling. *IEEE Trans. Commun.* **2020**, *68*, 6499–6513. [CrossRef]
22. Wang, Y.; Ciblat, P.; Serpedin, E.; Loubaton, P. Performance analysis of a class of nondata-aided frequency offset and symbol timing estimators for flat-fading channels. *IEEE Trans. Signal Process.* **2002**, *50*, 2295–2305. [CrossRef]
23. Dandawate, A.V.; Giannakis, G.B. Asymptotic theory of mixed time averages and kth-order cyclic-moment and cumulant statistics. *IEEE Trans. Inf. Theory* **1995**, *41*, 216–232. [CrossRef]
24. Gini, F.; Giannakis, G.B. Frequency offset and symbol timing recovery in flat-fading channels: A cyclostationary approach. *IEEE Trans. Commun.* **1998**, *46*, 400–411. [CrossRef]
25. Wang, Y.; Serpedin, E.; Ciblat, P. Blind feedforward cyclostationarity-based timing estimation for linear modulations. *IEEE Trans. Wirel. Commun.* **2004**, *3*, 709–715. [CrossRef]

26. Li, S.; Wang, S.; Zhao, C.; Cui, X.; Liu, J. A Non-Data-Aided Feedforward Timing Estimator Based on Multiple Cyclic Correlations for Short-Term Burst Signals. *IEEE Commun. Lett.* **2022**, *26*, 2166–2169. [CrossRef]
27. Sirbu, G.; Leonardi, M. Fully Autonomous Orbit Determination and Synchronization for Satellite Navigation and Communication Systems in Halo Orbits. *Remote Sens.* **2023**, *15*, 1173. [CrossRef]
28. Abd, M.H.; Al-Suhail, G.A.; Tahir, F.R.; Ali Ali, A.M.; Abbood, H.A.; Dashtipour, K.; Jamal, S.S.; Ahmad, J. Synchronization of Monostatic Radar Using a Time-Delayed Chaos-Based FM Waveform. *Remote Sens.* **2022**, *14*, 1984. [CrossRef]
29. Zhou, Z.; Yang, Y.; Ma, M.; Jiao, B. Distortion reduction in fractional delay filters. *IEEE Signal Process. Lett.* **2021**, *28*, 588–592. [CrossRef]

Disclaimer/Publisher's Note: The statements, opinions and data contained in all publications are solely those of the individual author(s) and contributor(s) and not of MDPI and/or the editor(s). MDPI and/or the editor(s) disclaim responsibility for any injury to people or property resulting from any ideas, methods, instructions or products referred to in the content.